



The Structural Basis of the Kinetic Mechanism of a Gap-Filling X-Family DNA Polymerase That Binds Mg^{2+} -dNTP Before Binding to DNA

Shuhei Nakane^{1,†}, Hirohito Ishikawa¹, Noriko Nakagawa^{1,2},
Seiki Kuramitsu^{1,2} and Ryoji Masui^{1,2*}

¹Department of Biological Sciences, Graduate School of Science, Osaka University, 1-1 Machikaneyama-cho, Toyonaka, Osaka 560-0043, Japan

²RIKEN SPring-8 Center, 1-1-1 Kouto, Sayo-cho, Sayo-gun, Hyogo 679-5148, Japan

Received 15 November 2011;
received in revised form
9 January 2012;
accepted 17 January 2012
Available online
27 January 2012

Edited by K. Morikawa

Keywords:

substrate-binding order;
Theorell–Chance mechanism;
crystal structure;
dNTP binding;
syn and *anti* conformations of
dGTP

DNA with single-nucleotide (1-nt) gaps can arise during various DNA processing events. These lesions are repaired by X-family DNA polymerases (PolXs) with high gap-filling activity. Some PolXs can bind productively to dNTPs in the absence of DNA and fill these 1-nt gaps. Although PolXs have a crucial role in efficient gap filling, currently, little is known of the kinetic and structural details of their productive dNTP binding. Here, we show that *Thermus thermophilus* HB8 PolX (ttPolX) had strong binding affinity for Mg^{2+} -dNTPs in the absence of DNA and that it follows a Theorell–Chance (hit-and-run) mechanism with nucleotide binding first. Comparison of the intermediate crystal structures of ttPolX in a binary complex with dGTP and in a ternary complex with 1-nt gapped DNA and Mg^{2+} -ddGTP revealed that the conformation of the incoming nucleotide depended on whether or not DNA was present. Furthermore, the Lys263 residue located between two guanosine conformations was essential to the strong binding affinity of the enzyme. The ability to bind to either *syn*-dNTP or *anti*-dNTP and the involvement of a Theorell–Chance mechanism are key aspects of the strong nucleotide-binding and efficient gap-filling activities of ttPolX.

© 2012 Elsevier Ltd. All rights reserved.

*Corresponding author. Department of Biological Sciences, Graduate School of Science, Osaka University, 1-1 Machikaneyama-cho, Toyonaka, Osaka 560-0043, Japan. E-mail address: rmasui@bio.sci.osaka-u.ac.jp.

† Research Fellow of the Japan Society for the Promotion of Science.

Present addresses: H. Ishikawa, Research Center for Asian Infectious Diseases, Institute of Medical Science, University of Tokyo, 4-6-1 Shirokanedai, Minato-ku, Tokyo 108-8639, Japan, and China–Japan Joint Laboratory of Structural Virology and Immunology, Institute of Biophysics, Chinese Academy of Sciences, 15 Datun Road, Beijing 100101, China.

Abbreviations used: ttPolX, X-family DNA polymerase of *Thermus thermophilus* HB8; POLXc, PolX core; PHP, polymerase and histidinol phosphatase; ttPolI, A-family DNA polymerase I of *T. thermophilus* HB8; RU, resonance unit; TdT, terminal deoxynucleotidyl transferase; Pol β , DNA polymerase β ; SPR, surface plasmon resonance; BSA, bovine serum albumin.

Introduction

Base excision repair is the major DNA repair pathway for dealing with damaged bases, such as the oxidized lesions that are associated with aging and the pathogenesis of many neurodegenerative disorders.¹ DNA with a single-nucleotide (1-nt) gap can arise during various DNA repair processes, especially base excision repair. Failure to deal with these gaps can cause serious damage to the DNA, such as strand breaks. Rapid and efficient filling of these gaps is carried out by X-family DNA polymerases (PolXs).

The African swine fever virus (ASFV) PolX is a highly distributive DNA polymerase² and follows an ordered Bi Bi mechanism with a nucleotide as the first substrate.³ This means that ASFV PolX can form a productive complex with a nucleotide in the absence of DNA and can, thereby, provide an effective means for filling 1-nt gaps. Terminal deoxynucleotidyl transferase (TdT), a mammalian PolX,⁴ follows a random Bi Bi mechanism;⁵ thus, it can also form a productive binary complex with a nucleotide. To date, however, the mechanism and order of binding and release of substrates and products have not been fully elucidated for these PolXs. By contrast with these DNA polymerases, the ordered Bi Bi mechanism with DNA as the first substrate is a conserved reaction mechanism for other DNA polymerases, especially replicative polymerases with high processivity. For example, the A-family DNA polymerase I (PolI) of *Escherichia coli* binds to DNA prior to binding to Mg^{2+} -dNTPs;⁶ PolI has low affinity for Mg^{2+} -dNTPs in the absence of DNA.⁷ Although PolI can bind to a nucleotide in the absence of DNA, this binary complex is nonproductive and must be dissociated before binding to DNA.⁸ DNA polymerase β (Pol β), a mammalian PolXs involved in base excision repair, has also been shown to follow an ordered Bi Bi mechanism with DNA as the first substrate, although these studies used primer/template and ~14-nt gapped DNA, which may not be the most appropriate substrates for PolXs.^{9,10} These differences in reaction mechanism among polymerases suggest the possibility that productive dNTP binding in the absence of DNA is responsible for the high activity of some PolXs, such as ASFV PolX, for filling 1-nt gaps.

The crystal structures of a few DNA polymerases in binary complexes with a nucleotide have been reported, for example, the Klenow fragment of *E. coli* PolI with dCTP,¹¹ *Thermus aquaticus* PolI with dCTP,¹² and Pol β with dATP.¹³ These binary structures lacked metal ions and the nucleotides had different binding positions and conformations compared to ternary complexes, which suggest nonproductive binding. These observations on

crystal structures are consistent with a polymerase mechanism of ordered Bi Bi with DNA as the first substrate. With respect to the crystal structure of TdT in binary complex with Co^{2+} -ddATP, the conformation and location of ddATP are similar to nucleotides in the ternary complexes of other PolXs.¹⁴ However, it is uncertain whether this binary complex structure is productive or not because the TdT reaction proceeds via a random Bi Bi mechanism.⁵ To date, the structure of a productive binary complex of dNTP and DNA polymerase with an ordered Bi Bi mechanism has not been elucidated.

Thermus thermophilus HB8 PolX (ttPolX) has DNA-dependent DNA/RNA polymerase and 3'-5' exonuclease activities; the active sites for these reactions are a PolX core (POLXc) and polymerase and histidinol phosphatase (PHP) domains, respectively.¹⁵ This type of PolX is widely distributed in bacteria. Here, we performed steady-state kinetic experiments and showed that ttPolX follows a Theorell–Chance mechanism;¹⁶ we also determined the crystal structures of the reaction intermediates for 1-nt gap filling. Our observations on mechanism and structures suggest a possible model for how ttPolX achieves efficient filling of 1-nt gaps.

Results

ttPolX has strong binding affinity for Mg^{2+} -dNTP in the absence of DNA

ttPolX is a highly distributive DNA polymerase that shows preferential activity for repair of 1-nt gaps over activity with primer/template DNA (Fig. 1). We found that ttPolX had little strand-displacement and misincorporation activity for 1-nt gapped DNA (Fig. 1b). Furthermore, ttPolX showed similar gap-filling activity for 1-nt gapped DNA in the absence and presence of 5'-phosphate (Fig. S1). This may be due to the lack of a basic residue at position of Asp64 in ttPolX (see Fig. S3c) as expected from a binding study in our previous report.¹⁵ Surface plasmon resonance (SPR) measurements showed that ttPolX had strong affinity for Mg^{2+} -dNTP, regardless of the identity of the base (Fig. 2 and Table 1). The binding affinity of ttPolX for Mg^{2+} -GTP was approximately 2 orders lower than that for Mg^{2+} -dGTP. Compared to ttPolX, *T. thermophilus* PolI (ttPolI) showed much lower binding affinity for Mg^{2+} -dGTP (Table 1), which may reflect the substrate-binding order of each polymerase. The strong binding affinity of ttPolX for Mg^{2+} -dNTPs may be related to its ability to form a productive binary complex with Mg^{2+} -dNTPs in the absence of DNA.

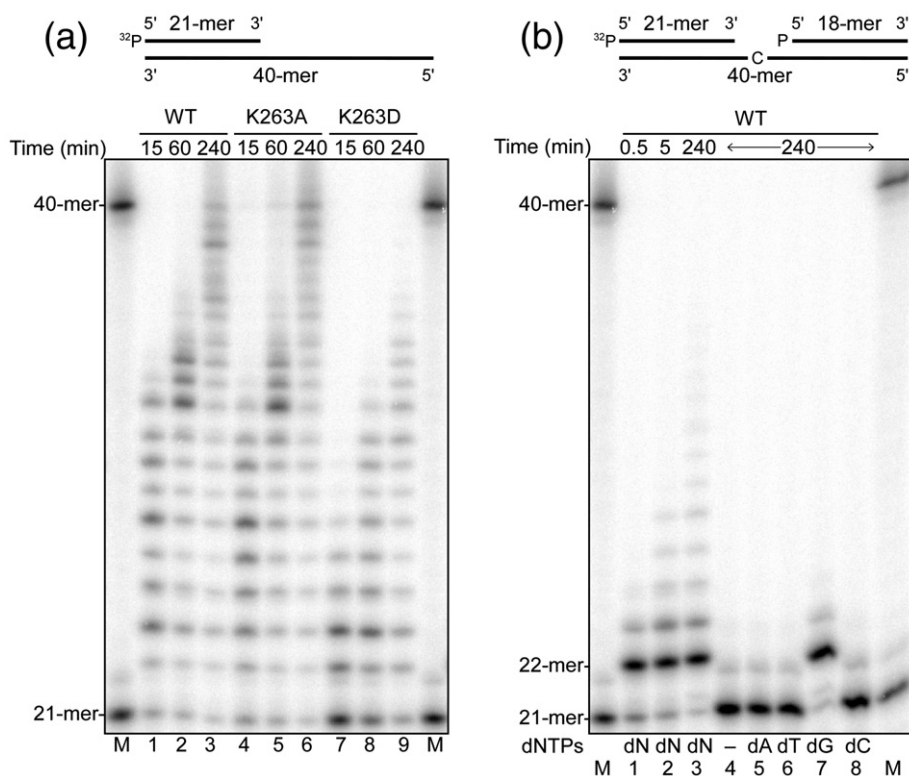


Fig. 1. DNA polymerase activity of ttPolX. (a) DNA polymerase activity for primer/template DNA. Reaction mixtures composed of 50 mM Tris-HCl, 20 mM KCl, 10 mM MgCl₂, 100 μg/ml BSA, 10 μM dNTPs, 10 nM primer/template DNA, and 1 μM ttPolX (wild type or mutants), pH 8.2, at 37 °C were incubated for the indicated times. (b) DNA polymerase activity for 1-nt gapped DNA. Reaction mixtures composed of 50 mM Tris-HCl, 20 mM KCl, 10 mM MgCl₂, 100 μg/ml BSA, 10 μM dNTP, 10 nM 1-nt gapped DNA, and 1 μM ttPolX wild type, pH 8.2, at 37 °C were incubated for the indicated times. Four-dNTP mixture (lanes 1–3) or single dNTP (lanes 5–8) was added to the reaction mixture. Lane 4 contained no dNTP. M represents marker lanes. The samples were analyzed by 20% (w/v) denaturing PAGE (8 M urea) and visualized by autoradiography using BAS2500 (Fuji Film).

Mechanism of 1-nt gap filling by ttPolX

To determine whether Mg²⁺-dNTP-bound ttPolX was productive, we investigated the ttPolX reaction mechanism using steady-state kinetics with dead-end and product inhibition (Fig. 3 and Table 2; Tables S1 and S2). First, the kinetic parameters for dGTP and DNA were determined in the absence of inhibitor (Fig. 3a and b; Table 2). The K_m value for dGTP (9.3 nM) was very low, as was the K_d value (12 nM) (Table 1). The K_m value for DNA (8.2 nM) was also low and was inconsistent with the K_d value (0.3 μM) obtained from an electrophoretic mobility shift assay in the absence of dNTP.¹⁵ Second, we performed the kinetic analysis using dCTP as a dead-end inhibitor to identify the order of substrate binding. ttPolX showed similar binding characteristics to Mg²⁺-dCTP and Mg²⁺-dGTP (Table 1) but did not incorporate dCTP against a dC template (Fig. 1b). Therefore, dCTP was a good dead-end inhibitor. dCTP exhibited competitive inhibition for variable

dGTP substrate (Fig. 3c) and had almost the same K_i (14 nM) as K_m for dGTP (Table 2). Moreover, dCTP exhibited mixed inhibition for variable DNA substrate (Fig. 3d). These results suggested that dNTP was the first substrate to bind (Table S1) because S_1 and S_2 were able to be interpreted as dGTP and DNA in Table S1, respectively. The inhibition constants of dCTP for variable DNA substrate were high because the fixed dGTP concentration (10 μM) was high (Table 2). We could not distinguish between “dNTP-first” ordered Bi Bi and rapid equilibrium random Bi Bi mechanisms by the dead-end inhibition pattern using dCTP (Table S1). We therefore examined the effect of the product inhibitor PPi and found competitive inhibition for variable dGTP substrate (Fig. 3e) and mixed inhibition for variable DNA substrate with an unsaturated dGTP concentration (Fig. 3f). These results support a dNTP-first ordered Bi Bi mechanism (Table 2 and Table S2), namely, dGTP, DNA, and PPi correspond to S_1 , S_2 , and P_2 in Table S2, respectively. Furthermore,

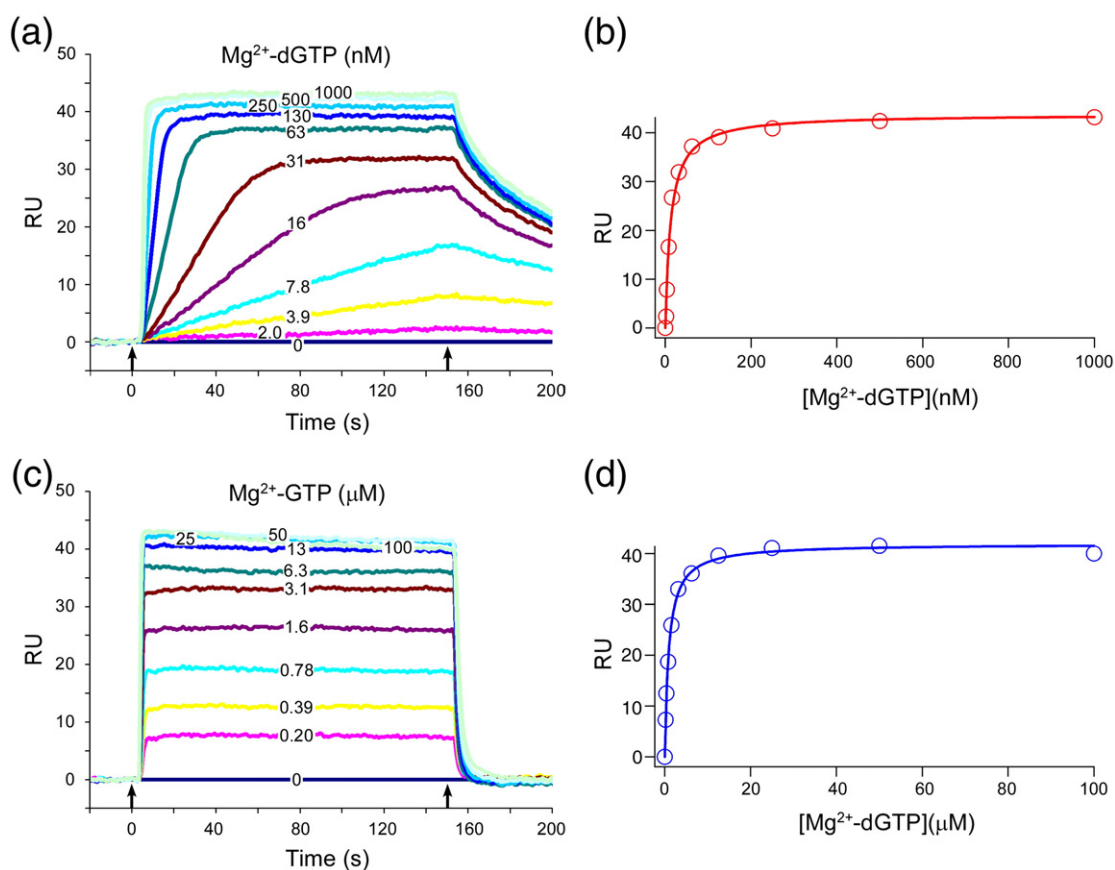


Fig. 2. SPR analysis of the binding affinity of ttPolX and nucleotides. (a) SPR sensorgrams of the binding of Mg²⁺-dGTP to ttPolX were obtained using the Biacore3000 system®. After equilibrating with running buffer, Mg²⁺-dGTP was passed over the chip at a flow rate of 100 μ l/min for 2.5 min (between arrowed points), followed by running buffer without dGTP, and then running buffer without Mg²⁺ to release nucleotides. (b) The averaged equilibrium points of RU were plotted against Mg²⁺-dGTP concentrations and fitted using Eq. (1) (see Materials and Methods). (c) SPR sensorgrams of the binding of Mg²⁺-GTP to ttPolX. (d) Averaged equilibrium points of RU were plotted against Mg²⁺-GTP concentrations.

the observation that PPi bound to ttPolX competitively with dGTP (Fig. 3e) indicated that PPi was released at the end of the reaction, a behavior pattern

Table 1. Dissociation constants (K_d) of *T. thermophilus* DNA polymerases and nucleotides determined by SPR analysis at 25 °C

	Analyte	n	K_d (nM)	
ttPolX	Wild type	Ca-dGTP	4	26±9.6
		Mg-dGTP	6	12±1.6
		Mg-dCTP	5	6.6±1.1
		Mg-dATP	4	6.9±1.1
		Mg-dTTP	6	24±1.8
		Mg-GTP	3	1100±190
		K263A	Mg-dGTP	4
K263D	Mg-dCTP	4	25±5.4	
	Mg-dGTP	4	260±25	
	Mg-dCTP	4	220±17	
ttPolI	Mg-dGTP	6	87,000±18,000	

Data represent the means of replicate experiments (n)±standard deviation.

that differs from other DNA polymerases.^{6,9,10} Finally, we used the other product, nicked DNA, as the inhibitor (P_1 in Table S2) in order to further test the hypothesis of a dNTP-first ordered Bi Bi mechanism. Interestingly, nicked DNA exhibited mixed inhibition for variable dGTP substrate with an unsaturated DNA concentration (Fig. 3g) and competitive inhibition for variable DNA substrate (Fig. 3h and Table 2). This inhibition pattern is consistent with a Theorell-Chance mechanism (Table S2), which is a special type of ordered Bi Bi mechanism. This reaction mechanism indicates that the steady-state concentrations of the ternary complexes were very low under the conditions used in the gap-filling assays with ttPolX and that dNTP-bound ttPolX reacted with 1-nt gapped DNA in a “hit-and-run” fashion (see Fig. 10). Because of this property, nicked DNA, which is the first-released product, competitively inhibited 1-nt gapped DNA, which is the second-binding substrate (Fig. 3h and Table S2). If the mechanism

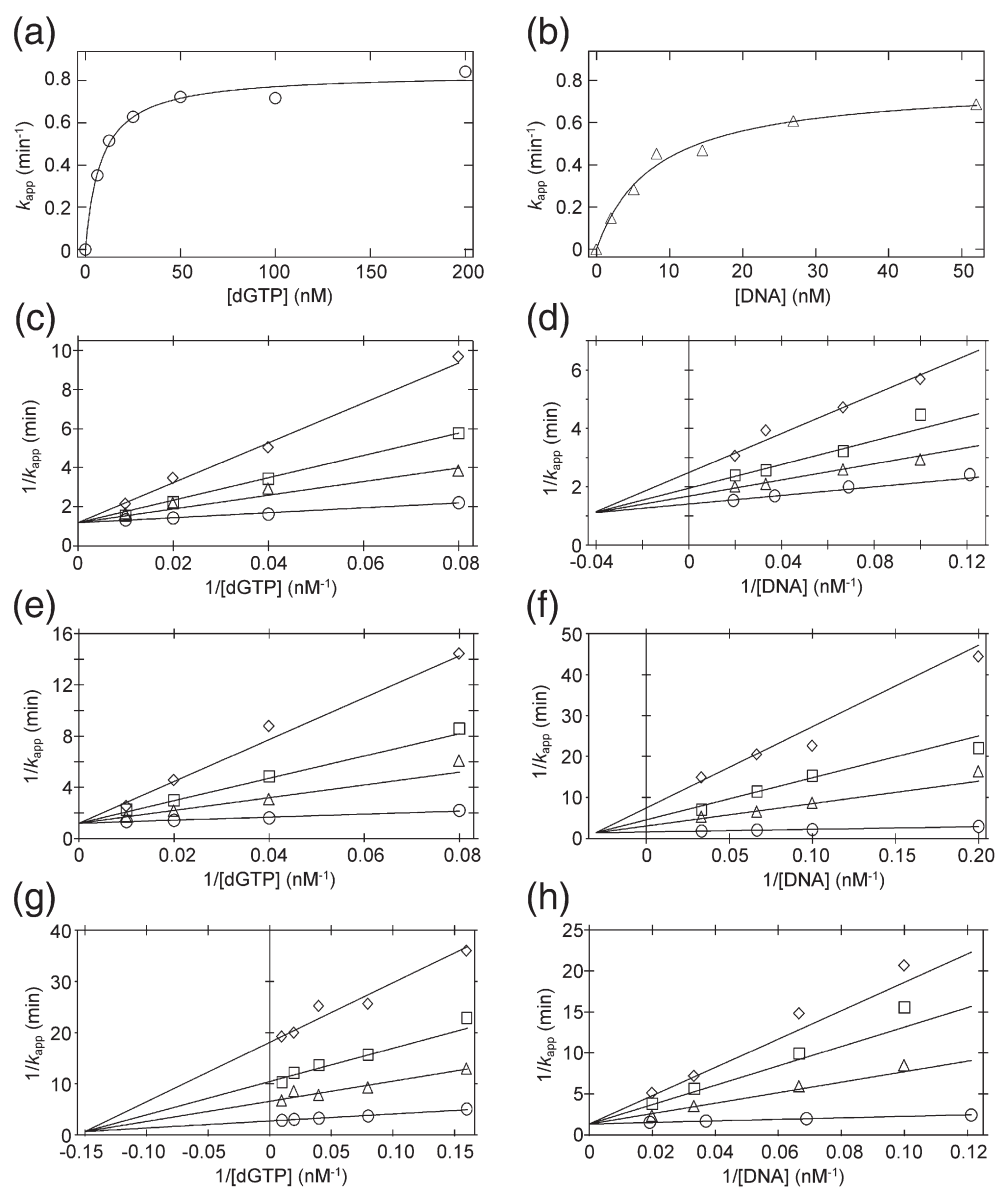


Fig. 3. Dead-end and product inhibition of wild-type ttPolX for 1-nt gap filling with dGTP. Reaction mixtures were composed of 50 mM Tris-HCl, 100 mM KCl, 10 mM MgCl₂, 100 μg/ml BSA, dGTP, 1-nt gapped DNA, and 0.5–1 nM ttPolX wild type, pH 7.5, at 37 °C. (a) dGTP concentration dependence of k_{app} with a fixed concentration of DNA (100 nM). The data were fitted with Eq. (2), described in the Materials and Methods, to obtain the steady-state kinetic parameters k_{cat} and K_m . (b) DNA concentration dependence of k_{app} with a fixed concentration of dGTP (10 μM). (c) Double-reciprocal plots for dead-end inhibition assays with a fixed concentration of DNA (100 nM) and various concentrations of dGTP in the presence of 0 nM (○), 25 nM (△), 50 nM (□), and 100 nM (◇) dCTP as the mismatched substrate. (d) Double-reciprocal plots for dead-end inhibition assays with a fixed concentration of dGTP (10 μM) and various concentrations of DNA in the presence of 0 μM (○), 5 μM (△), 10 μM (□), and 20 μM (◇) dCTP. (e) Double-reciprocal plots for product inhibition assays with 100 nM DNA and various concentrations of dGTP in the presence of 0 μM (○), 50 μM (△), 100 μM (□), and 200 μM (◇) PPI. (f) Double-reciprocal plots for product inhibition assays with an unsaturated concentration of dGTP (12.5 nM) and various concentrations of DNA in the presence of 0 μM (○), 50 μM (△), 100 μM (□), and 200 μM (◇) PPI. (g) Double-reciprocal plots for product inhibition assays with an unsaturated concentration of DNA (10 nM) and various concentrations of dGTP in the presence of 0 μM (○), 1 μM (△), 2 μM (□), and 4 μM (◇) nicked DNA. (h) Double-reciprocal plots for product inhibition assays with 10 μM dGTP and various concentrations of DNA in the presence of 0 μM (○), 2 μM (△), 4 μM (□), and 6 μM (◇) nicked DNA.

Table 2. Inhibition patterns and steady-state kinetic parameters of wild-type *ttPolX* for 1-nt gap filling with dGTP

Inhibitor	Variable substrate	Fixed substrate	Inhibition pattern	k_{cat} (min^{-1}) ^a	K_m (nM) ^a	K_i (μM) ^a	K_i' (μM) ^a
None	dGTP	DNA		0.83 ± 0.11^b	9.3 ± 1.4^b		
	DNA	dGTP		0.77 ± 0.078^c	8.2 ± 0.31^c		
dCTP	dGTP	DNA	Competitive	0.85 ± 0.034	11 ± 1.9	0.014 ± 0.0023	
	DNA	dGTP	Mixed	0.73 ± 0.017	6.3 ± 0.60	7.3 ± 1.3	24 ± 2.9
PPi	dGTP	DNA	Competitive	0.84 ± 0.022	10 ± 1.1	16 ± 1.5	
	DNA	dGTP (unsaturation) ^d	Mixed	0.62 ± 0.012	4.0 ± 0.31	6.8 ± 0.80	56 ± 9.6
Nicked DNA	dGTP	DNA (unsaturation) ^d	Mixed	0.37 ± 0.0054	5.1 ± 0.36	0.53 ± 0.095	0.69 ± 0.035
	DNA	dGTP	Competitive	0.76 ± 0.023	7.1 ± 0.84	0.35 ± 0.033	

^a Errors associated with global fitting are shown as standard deviations.

^b Means of 4 experiments \pm standard deviations.

^c Means of 5 experiments \pm standard deviations.

^d Unsaturated concentrations of substrates were determined by their K_m values.

was a dNTP-first ordered Bi Bi, nicked DNA is expected to show mixed inhibition against 1-nt gapped DNA substrate (Table S2). The Theorell–Chance mechanism may be advantageous for filling 1-nt gaps.

ttPolX can form both *syn*-dGTP and *anti*-dGTP binary complexes

Next, we investigated the implications of a Theorell–Chance mechanism on the crystal structures

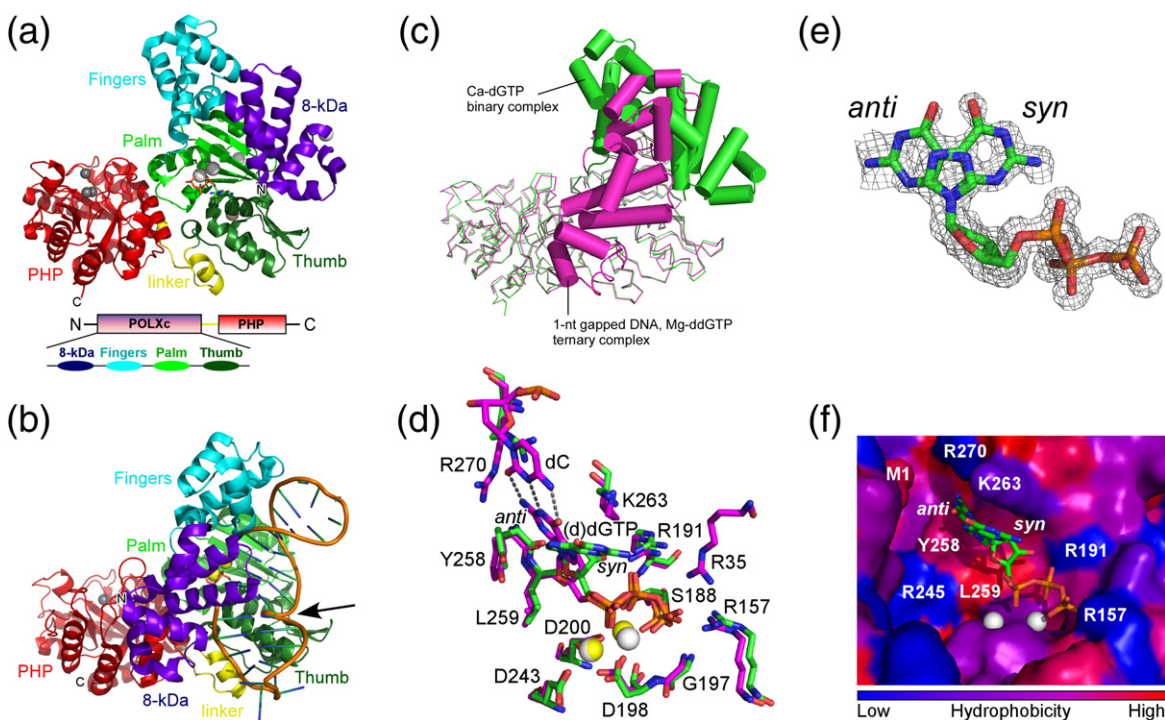


Fig. 4. Overall and active-site structures of the binary and ternary complexes. (a) The binary complex of *ttPolX* and Ca^{2+} -dGTP has four POLXc subdomains [8-kDa (purple blue, residues 1–87), fingers (cyan, 88–157), palm (light green, 158–247), thumb (dark green, 248–316)], linker (yellow, 317–335), and PHP (red, 336–575) (see also Fig. 5)]. (b) The ternary complex of *ttPolX* with 1-nt gapped DNA and ddGTP. The black arrow indicates the template strand bend. (c) Superposition of the binary (green) and ternary (magenta) complexes of (a) and (b). The DaliLite program²¹ was used to perform superposition of the palm and thumb subdomains. The cylinders in the 8-kDa and fingers subdomains represent α -helices. (d) Superposition of the polymerase active-site residues shown in (c). (e) The $F_{\text{obs}} - F_{\text{calc}}$ omit map of dGTP in the wild-type binary complex is contoured at 2σ as a gray mesh. (f) Hydrophobicity and surface profiles of the active site of the binary complex. Red and blue indicate hydrophobic and hydrophilic regions, respectively. Amino acid hydrophobicity is colored in accordance with the normalized consensus hydrophobicity scale.⁶⁵ White, yellow, and gray spheres are Ca^{2+} , Mg^{2+} , and Zn^{2+} ions, respectively. *syn* and *anti* conformations of dGTP in the binary complex are shown in superposition in (e) and (f).

Table 3. Data collection and refinement statistics

	Wild-type Ca-dGTP (binary complex)	Selenomethionine (Ca-dGTP)	Primer/template DNA + ddGTP	1-nt gapped DNA + ddGTP (ternary complex)	K263A mutant (Ca-dGTP)	K263D mutant (Ca-dGTP)	
<i>Data collection^a</i>							
X-ray source	BL26B2 at SPring-8	BL26B2 at SPring-8	BL26B2 at SPring-8	BL26B2 at SPring-8	BL26B2 at SPring-8	BL26B2 at SPring-8	
Space group	$P2_1$	$P2_1$	$P4_32_12$	$P2_12_12_1$	$P2_1$	$P2_1$	
Cell dimensions							
<i>a</i> , <i>b</i> , <i>c</i> (Å)	69.2, 53.3, 84.9	68.6, 54.5, 85.0	80.2, 80.2, 268.6	95.4, 96.9, 143.4	69.1, 53.2, 84.9	68.9, 53.2, 84.9	
α , β , γ (°)	90.0, 107.5, 90.0	90.0, 105.2, 90.0	90.0, 90.0, 90.0	90.0, 90.0, 90.0	90.0, 107.7, 90.0	90.0, 107.7, 90.0	
		Peak	Inflection				
Wavelength	1.000	0.9790	0.9793	1.000	1.000	1.000	
Resolution (Å)	50–1.40 (1.42–1.40)	50–1.80 (1.86–1.80)	50–1.80 (1.86–1.80)	50–3.3 (3.42–3.3)	50–2.70 (2.75–2.70)	50–1.36 (1.38–1.36)	50–1.45 (1.48–1.45)
R_{merge}	0.043 (0.256)	0.079 (0.328)	0.077 (0.512)	0.065 (0.2)	0.136 (0.567)	0.044 (0.258)	0.040 (0.322)
$I/\sigma I$	52.2 (6.6)	34.3 (5.7)	31.7 (3.6)	36.7 (6.2)	15.6 (3.5)	26.6 (4.0)	29.1 (3.1)
Completeness (%)	98.5 (97.2)	99.7 (99.4)	99.7 (99.7)	99.3 (98.1)	100 (100)	99.6 (99.6)	99.7 (100)
Redundancy	7.5 (6.8)	7.1 (6.2)	6.9 (5.6)	11.5 (7.7)	7.4 (7.3)	3.7 (3.6)	3.7 (3.7)
<i>Refinement</i>							
Resolution (Å)	80.94–1.40			76.82–3.30	50.0–2.70	50.0–1.36	50–1.45
No. of reflections	108,638			13,885	37,064	118,839	98,308
$R_{\text{work}}/R_{\text{free}}$	0.162/0.188			0.256/0.319	0.241/0.293	0.171/0.198	0.175/0.205
No. of atoms							
Protein	4531			4425	9001	4536	4539
DNA	0			346	1178	0	
Ligand/ion	39			42	66	38	37
Water	622			26	134	551	521
<i>B</i> -factors							
Protein	20.8			83.8	33.1	19.7	20.7
DNA				79.8	44.8		
Ligand/ion	18.2			80.0	15.1	15.9	16.7
Water	30.7			45.2	22.7	27.1	28.1
r.m.s.d							
Bond lengths (Å)	0.011			0.014	0.006	0.010	0.012
Bond angles (°)	1.38			1.63	1.14	1.38	1.50
Ramachandran plot (%)							
Most favored	93.7			82.8	90	93.3	92.7
Additional allowed	5.9			16.1	9.1	6.3	6.7
Generously allowed	0.4			1	0.9	0.4	0.6
Disallowed	0			0	0	0	0
Protein Data Bank ID	3AU2			3AU6	3AUO	3BOX	3BOY

Values in parentheses are for the highest-resolution shell.

^a One crystal was used for each data set.

associated with ttPolX. We compared the crystal structures of ttPolX with Ca^{2+} -dGTP at 1.4 Å (binary complex) against 1-nt gapped DNA and Mg^{2+} -ddGTP at 2.7 Å (ternary complex) (Fig. 4a and b; Table 3). These two complexes are thought to be the first and second intermediates of the ttPolX gap-filling reaction pathway. ttPolX has POLXc and PHP domains; these domains have also been identified in the crystal structure of *Deinococcus radiodurans* PolX.¹⁷ The POLXc domain has four subdomains: 8-kDa, fingers, palm, and thumb (Figs. 4a and b and 5). Two Ca^{2+} ions, derived from the crystallization reagent, were present in the polymerase active site of the binary complex (Fig. S2). The binding affinities for Ca^{2+} -dGTP and Mg^{2+} -dGTP were similar despite the fact that Ca^{2+} is not an active cofactor for the polymerase activity of ttPolX (Table 1). The 8-kDa subdomain bound to downstream DNA and 1-nt gapped DNA was bent (Fig. 4b, black arrow, and Fig. S3). These two binary and ternary complexes showed good superposition in the palm, thumb, and PHP domains (Fig. 4c). The N-terminal 8-kDa and fingers subdomains were shifted by binding to DNA, implying N-terminal flexibility (Fig. 4c and Fig. S3).

Comparison of the active sites in the binary and ternary complexes showed that they have similar structures (Fig. 4d). The site for polymerase activity in ttPolX has three conserved Asp residues (D198, D200, and D243) and two metal ions, similar to Polβ (Fig. 6a), indicating that ttPolX has the standard two-metal-ion mechanism for polymerase activity. We found that dGTP conformations were different between the binary and ternary complexes (Fig. 4d). The spatial relationship between ribose and the nucleoside base can be classified into *syn* or *anti* conformations. Under the International Union of Pure and Applied Chemistry definition, the conformation is deemed to be *syn* when the N-glycosidic angle χ of the nucleoside is $0 \pm 90^\circ$ and to be *anti* when the angle is $180 \pm 90^\circ$. We found an N-glycosidic angle of 77.17° for dGTP in the binary complex (i.e., a *syn* conformation). In contrast, the incoming ddGTP in the ternary complex was in the *anti* conformation, like all nucleotides in A- and B-DNA (Fig. 4d). This difference was also observed when we compared the binary complex of ttPolX with the ternary complexes of Polβ with 1-nt

gapped DNA or with ttPolX with primer/template DNA (Fig. 6 and Fig. S3). Detailed analysis of the residual density map revealed that the dGTP in the binary complex was also in the *anti* conformation (Fig. 4e) and its glycosidic angle was similar to that of ddGTP (*anti*) in the ternary complex (Fig. 4d). Assuming that the crystallographic B-factors are the same in both *syn* and *anti* conformations of dGTP, occupancy of *syn* and *anti* conformations was approximately 0.64 and 0.36, respectively. Thus, the conformation of the nucleotides changed from *syn* to *anti* in the presence of DNA. It is possible that the binding to nucleotides in the *syn* conformation may be related to the strong and productive binding in the absence of DNA.

Lys263 controls binding affinity and conformation of dGTP

Mutational studies indicated that Lys263 was essential for the strong binding to Mg^{2+} -dNTPs (Table 1). Lys263 is located between the bases of *syn*-dGTP and *anti*-dGTP and appears to stack with bases in the *syn* conformation (Fig. 4d and f). The K263A and K263D mutants had a 4- to 20-fold lower binding affinity, respectively, for Mg^{2+} -dNTP than the wild-type enzyme. The positive charge on the long side chain of Lys at this position may provide additional stabilization of Mg^{2+} -dNTPs compared to Ala. Lysine (or a similar residue) is widely conserved at this position in ttPolX, for example, bacterial and archaeal PolXs, human DNA polymerase μ (Lys438), and human TdT (Arg453)²² (Fig. 5b). This conservation implies that strong binding to Mg^{2+} -dNTPs is a common strategy among PolXs. The observation that a negatively charged residue at this position (Asp263 in the K263D mutant) weakened the binding affinity for Mg^{2+} -dNTPs is consistent with the mutation analysis of Polβ.²³ Polβ has an Asp at this position and is thus different from other PolXs (Fig. 5b), although its other active-site residues are similar to those of ttPolX (Fig. 6a). The residue at position 263 may control binding affinity for Mg^{2+} -dNTPs and thus may provide different properties among PolXs with respect to processivity, selectivity, and substrate-binding order.

Fig. 5. Sequence alignments of POLXc domains of representative PolXs. (a) Alignment of the 8-kDa and fingers subdomains. (b) Alignment of the palm and thumb subdomains. Residues in white and highlighted in black show the important residues for the *syn-anti* equilibrium of the incoming nucleotide. Residues in black and highlighted in white show stacking residues around the bend. The abbreviations are as follows: ttPolX, *T. thermophilus* HB8 PolX; bsPolX, *Bacillus subtilis* PolX; drPolX, *D. radiodurans* PolX; hsPolβ, *H. sapiens* Polβ; hsPolλ, *H. sapiens* Polλ; hsPolμ, *H. sapiens* Polμ; hsTdT, *H. sapiens* terminal deoxynucleotidyl transferase; ASFV PolX, African swine fever virus PolX. The sequence accession numbers are as follows: YP_144416 for ttPolX, NP_390737 for bsPolX, NP_294190 for drPolX, NP_002681 for hsPolβ, NP_037406 for hsPolλ, NP_037416 for hsPolμ, NP_004079 for hsTdT, and NP_042790 for ASFV PolX. Sequence domains are highlighted using the same color scheme as in Fig. 4. Multiple alignments were calculated by ClustalW2¹⁸ and displayed by ESPript.¹⁹ The represented secondary structure derives from the ttPolX binary complex. The notations in the figure are as follows: α, α-helix, β, β-sheet, TT, strict β-turn, and η, 3_{10} helix.

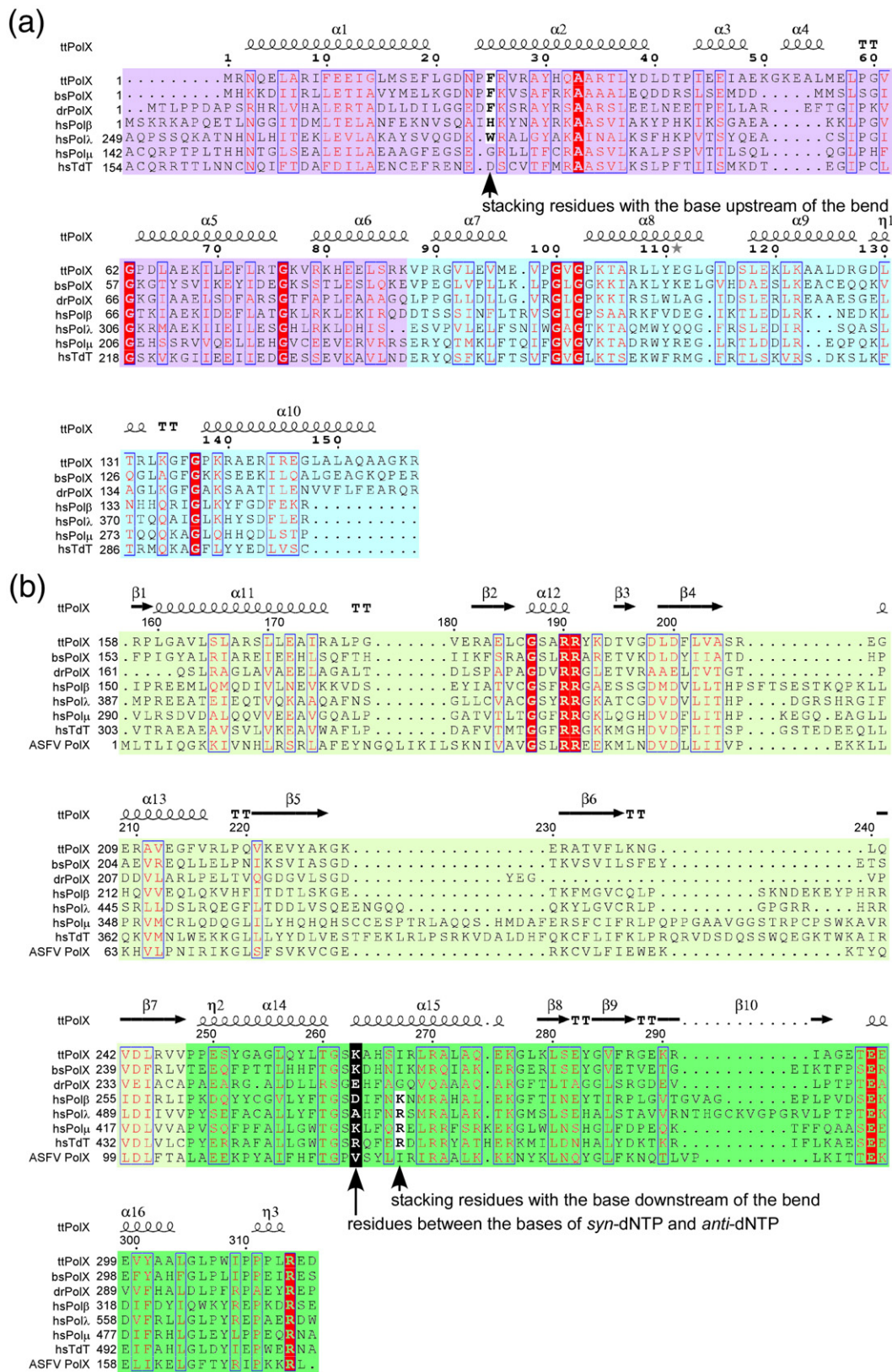


Fig. 5 (legend on previous page)

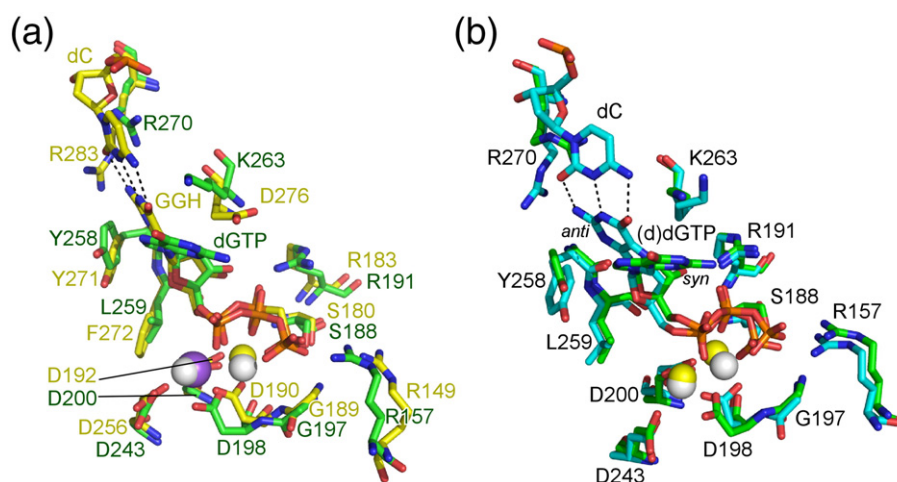


Fig. 6. Comparison of the polymerase active sites of the *ttPolX* binary complex and of ternary complexes. (a) Superposition of the polymerase active sites of the *ttPolX* binary complex (green) and the *Polβ* ternary complex (yellow). The structure of the *Polβ* ternary complex contains 1-nt gapped DNA and a dGTP analog, 2'-deoxyguanosine 5'- β , γ -methylene triphosphate.²⁰ The residues and residue numbers are shown as green (*ttPolX* binary complex) and yellow (*Polβ*). The DaliLite program²¹ was used to perform the structure superposition of the palm and thumb subdomains. (b) Superposition of the polymerase active sites of the *ttPolX* binary complex (green) and the complex with primer/template and ddGTP (Fig. S3) (cyan). White, yellow, and purple spheres are Ca^{2+} , Mg^{2+} , and Na^{+} ions, respectively.

We compared the *ttPolX* crystal structures of wild type, K263A, and K263D mutants in complex with Ca^{2+} -dGTP (Table 3). The three structures were similar except for residue 263 and dGTP conformation (Fig. 7a). In the wild-type structure, Lys263 had higher average *B*-factors (24.2 \AA^2 , side chain) than

other active-site residues. Because the *B*-factor in crystal structures reflects the fluctuation of an atom,²⁴ the large *B*-factor of the side chain of Lys263 implies that this side chain had high mobility and did not prevent conformational change of dGTP (Fig. 4e and f). dGTP bound to K263A was in the *anti*

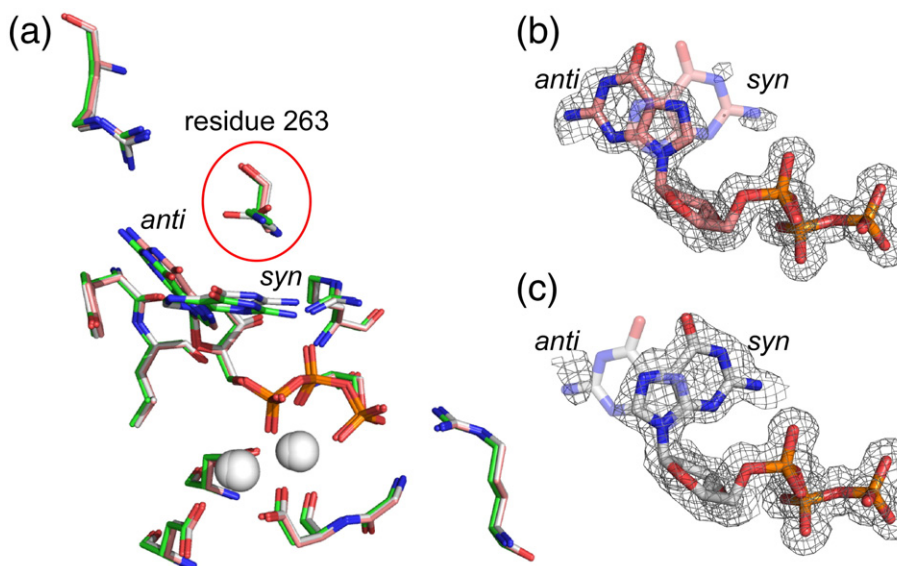


Fig. 7. Structure of the polymerase active sites of Lys263 mutants. (a) Superposition of the polymerase active-site residues of the wild type (green), K263A (pink), and K263D (white) binary complexes. dGTPs are shown as *syn* and *anti* (wild type), *anti* (K263A), and *syn* (K263D) conformations. White spheres are Ca^{2+} ions. (b) The $F_{\text{obs}} - F_{\text{calc}}$ omit map of dGTP in the K263A structure is contoured at 2σ as a gray mesh. Electron density was clearly observed for *anti*-dGTP but not for *syn*-dGTP; the latter is displayed with a semitransparent appearance. (c) The $F_{\text{obs}} - F_{\text{calc}}$ omit map of dGTP in the K263D structure is contoured at 2σ as a gray mesh. Electron density was clearly observed for *syn*-dGTP but not for *anti*-dGTP; the latter is displayed with a semitransparent appearance.

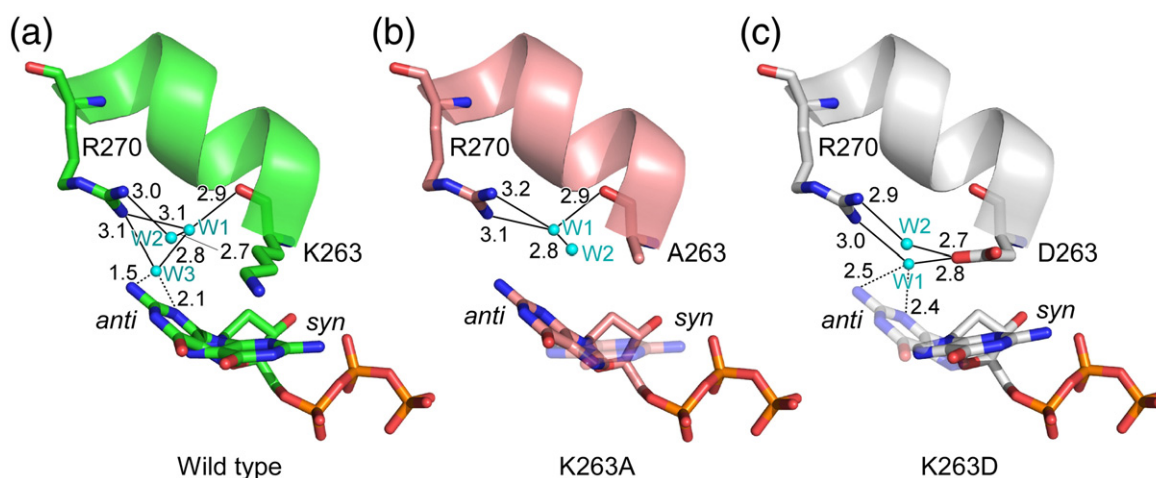


Fig. 8. Arrangement of water molecules around *anti*-dGTPs. Three water molecules (W1, W2, and W3) are present around *anti*-dGTPs of wild type (a), K263A (b), and K263D (c) structures; water molecules are shown in cyan. Continuous lines represent hydrogen bonds within a 3.2-Å diameter around the water molecules. Broken lines represent clashes (wild type) or possible hydrogen bonds (K263D) with *anti*-dGTP. The numbers along the lines represent distances in angstroms. W3 can only be placed when *anti*-dGTP is not present, because the distance between W3 and *anti*-dGTP is otherwise too short (≤ 2.2 Å). *syn*-dGTP and *anti*-dGTP are shown as semitransparent in the K263A and K263D structures, respectively.

conformation (Fig. 7a and b). dGTP bound to K263D appeared to be prevented from flipping by Asp263 and was in the *syn* conformation (Fig. 7a and c). Moreover, Asp263, together with Arg270, stably held two water molecules (W1 and W2) (Fig. 8c). These two water molecules were also held by Arg270 and the main chain of Lys263 in the wild type (Fig. 8a), but there were fewer and longer hydrogen bonds between the wild type and two water molecules (W1 and W2, hydrogen-bonding distances of 3.1, 3.0, and 2.9 Å) compared to K263D (hydrogen-bonding distances of 3.0, 2.9, 2.8, and 2.7 Å). K263A also had two water molecules; however, the hydrogen bond between W2 and ttPolX was absent in K263A (Fig. 4b). Furthermore, W3 in the wild type and W1 in the K263D were close to *anti*-dGTP (Fig. 8a and c). These differences may affect the hydrophilic environment around *anti*-dGTP. The hydrophobic guanine moiety of *anti*-dGTP may be rejected by the hydrophilic environment in the absence of DNA in the wild-type and K263D structures (Fig. 8a and c). When DNA was bound, the bound dNTP was in the *anti* conformation, Arg270 was directed to the other side, and the water molecules held by Arg270 were released (Fig. 4d). In the K263A structure, there was a weak hydrophilic environment around the *anti*-dGTP and no obvious interaction between Ala263 and *syn*-dGTP (Fig. 8b). Moreover, Tyr258 may provide hydrophobic environment around *anti*-dGTP (Fig. 4d and f). The *syn*-*anti* equilibrium may be biased towards *anti* in the K263A structure by these factors. Taken together, our observations indicate that Lys263 may flexibly control the *syn*-*anti* equilibrium of dGTP bound to ttPolX.

Influence of residue 263 on the kinetic mechanism for filling 1-nt gaps

Since Lys263 mutants had a different binding strategy for dGTP and lower binding affinity than the wild type (Fig. 8 and Table 1), we examined the reaction mechanism of the mutants (Figs. S4 and S5; Tables S3 and S4). Both K263A and K263D showed distributive polymerase activity similar to that of the wild type (Fig. 1a). The K_m value for dGTP was increased in both mutants (K263A, 24 nM; K263D, 260 nM); however, the K_m for DNA of K263A (11 nM) was similar to that of the wild type, whereas that of K263D was slightly increased (41 nM), indicating that residue 263 was not involved in DNA binding. The k_{cat} and K_m values for DNA of K263A (0.89 min^{-1} and 11 nM) were similar to those of the wild type (0.77 min^{-1} and 8.2 nM) (Fig. S4; Table 2 and Table S3). Thus, the *anti*-dGTP (Fig. 8b) did not prevent DNA binding and catalysis. The decrease of k_{cat} of K263D (0.48 min^{-1} for dGTP and 0.46 min^{-1} for DNA) (Fig. S5; Table 2; Table S4) may indicate that the conformational change of the incoming nucleotide from *syn* to *anti* was directly involved in the catalysis step. The kinetic differences between the wild type and mutants suggest that the ability of Lys263 to bind to both *syn*- and *anti*-dGTP contributed to the binding affinity for Mg^{2+} -dGTP without decreasing the k_{cat} value (Table 2; Tables S3 and S4).

The decreased binding affinity of the mutants for Mg^{2+} -dNTP raised the possibility that the substrate-binding order was altered by mutation of residue 263. However, dead-end and product inhibition assays revealed that the reaction mechanism for

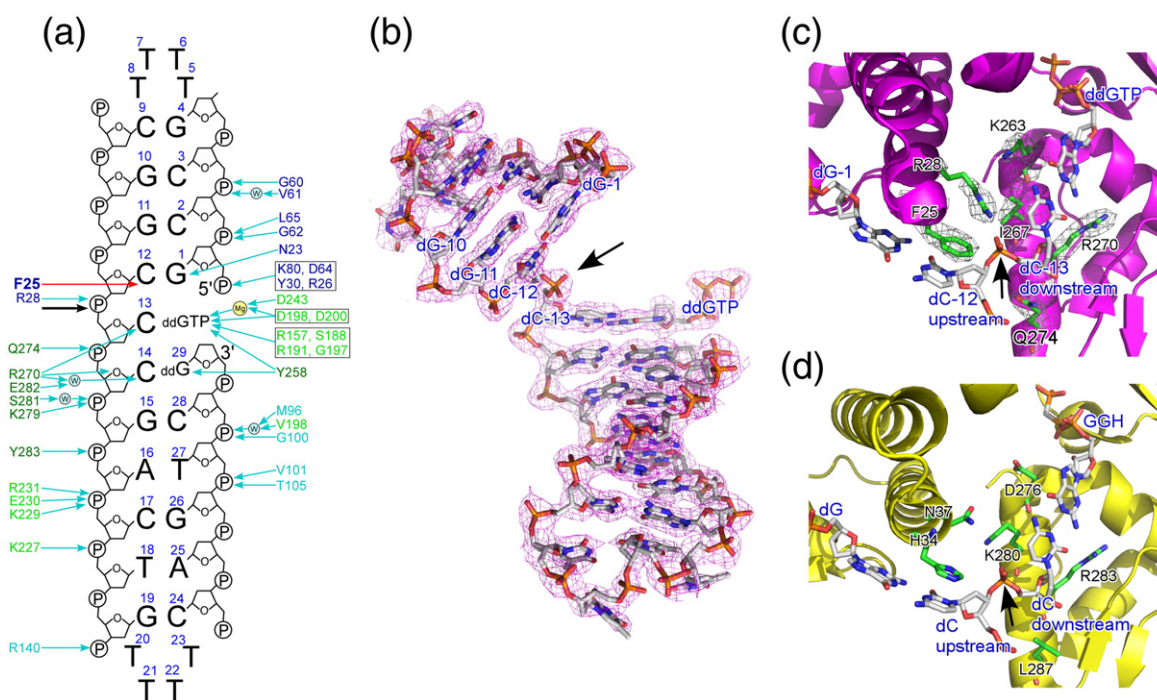


Fig. 9. DNA-binding residues of the ttPolX ternary complex with 1-nt gapped DNA. (a) Interaction between ttPolX, gapped DNA, and Mg^{2+} -ddGTP. Residue numbers are colored as in Fig. 2b. Cyan arrows indicate hydrogen bonds ($\leq 3.2 \text{ \AA}$); red arrows indicate nonbonded interactions; W, water molecules; P, DNA backbone phosphates; Mg, magnesium ion (Mg^{2+}). DNA residue numbers are shown in blue. (b) 1-nt gapped DNA and Mg^{2+} -ddGTP. A $2F_{\text{obs}} - F_{\text{calc}}$ electron density map contoured at 1σ is shown in magenta. (c) The DNA-interacting residues of the ttPolX ternary complex with 1-nt gapped DNA around the template strand bend. DNA residues and protein residues are shown as white and green, respectively. A $2F_{\text{obs}} - F_{\text{calc}}$ electron density map contoured at 1σ is shown in gray. (d) The DNA-interacting residues of the Pol β ternary complex with 1-nt gapped DNA²⁰ around the template strand bend. Black arrows in (a)–(d) indicate the template strand bend.

filling 1-nt gaps of the mutants was similar to that of the wild type (Figs. S4 and S5; Tables S3 and S4). The K_i values of dCTP were increased in proportion to the K_m for dGTP, because ttPolX bound to Mg^{2+} -dCTP with almost the same affinity as to Mg^{2+} -dGTP (Table 1). The inhibition constants of the mutants for PPi and nicked DNA were similar to those of the wild type (Tables S3 and S4). Therefore, it was likely that residue 263 was involved in the interaction between ttPolX and the base of incoming nucleotide.

DNA-binding residues of ttPolX

It is possible that other residues, in addition to residue 263, are involved in determining the substrate-binding order. Pol β has an Asp at the corresponding position to 263 of ttPolX and follows a DNA-first ordered Bi Bi mechanism.¹⁰ However, the K263D mutant of ttPolX retained the dNTP-first binding order (Table S4), although the binding affinity for Mg^{2+} -dNTP in the absence of DNA was much lower than that of wild type (Table 1). This difference is consistent with a role for other

residues also determining substrate-binding order through interaction with the incoming nucleotide or DNA. In ttPolX and Pol β , the residues interacting with the incoming nucleotides are similar except for residue 263 in ttPolX (Fig. 6a). Therefore, the residues involved in DNA binding seem also to have a role in substrate-binding order in PolXs. The number of interactions between ttPolX and 1-nt gapped DNA was similar to other PolXs (Fig. 9a). However, the interaction around the template strand bend (Fig. 9a and b) differed (Fig. 9c and d). The Phe25 in the 8-kDa subdomain has a stacking interaction with dC-12, which is upstream of the bend in the template strand (Fig. 9a and c). This stacking residue is conserved in many bacterial and archaeal PolXs (Fig. 5a and Fig. 1 of Banos *et al.*).²² An aromatic residue is also found at this position in *Homo sapiens* Pol β (hsPol β) (His34) (Fig. 9d) and hsPol λ (Trp274), but not in hsPol μ (Gly174) or hsTdT (Asp186) (Fig. 5). Eukaryotic PolXs also have stacking interactions with the base downstream of the bend (Fig. 9d) (e.g., hsPol β Lys280, hsPol λ Arg514, hsPol μ Arg442, and hsTdT Arg457). However, this stacking residue is not conserved in ttPolX

(Ile267) (Fig. 9c) and in bacterial and archaeal PolXs (Fig. 5b).²² hsPol β and hsPol λ have two stacking residues near the bend position; however, hsPol μ , hsTdT, and bacterial and archaeal PolXs have only one stacking residue. This difference may be related to the affinity for gapped DNA, substrate-binding order, and efficiency of filling gaps larger than 2 nt.²⁵

Discussion

Productive binding with dNTP in the absence of DNA

The observation that both *syn* and *anti* conformations of dGTP can occur in the binary complex (Fig. 4e) suggests that the bound nucleotide can change its conformation even in ttPolX. The ability to switch its nucleotide-binding property may depend on Lys263 (Figs. 4, 7, and 8). This ability may be advantageous from an entropic point of view and contribute to strong nucleotide binding in the absence of DNA (Table 1). Furthermore, the *syn-anti* equilibrium also allows DNA to be bound without release of Mg²⁺-dNTPs since the *anti*-dNTPs can base pair directly with a template base (Fig. 4d and Table 2). NMR analysis showed that Mg²⁺-dATP and Mg²⁺-TTP bound to bacterial PolI had the *anti* conformation.²⁶ At the location corresponding to Lys263 of ttPolX, PolIs have aromatic residues that stack with incoming *anti*-dNTPs but not with *syn*-dNTPs.^{27,28} Since the PolI-dNTP binary complex is thought to be nonproductive,⁸ the two binary complexes with *syn*-dNTP and *anti*-dNTP achieved by Lys263 may be important for a strong and productive complex in the absence of DNA. However, K263A and K263D mutants still retained the dNTP-first binding order (Tables S3 and S4). As described earlier, residues other than Lys263 may also be involved in substrate-binding order.

Nucleotide conformations of *syn* and *anti*

This study has identified the important role played by the *syn-anti* conformational change of the incoming nucleotide in the active site of ttPolX. Spectroscopic analysis showed that nucleosides rapidly achieve a *syn-anti* equilibrium in solution.^{29–32} This *syn-anti* equilibrium is affected by sugar puckering and modifications.^{33–35} The phosphorylation of O5' increases the interaction between O5' and a base, which increases C3'-*endo* in sugar puckering, followed by an increase of the *anti* conformation.^{36,37} In guanine nucleotides, the interaction between the amino group at the C2-position and the 5'-phosphate stabilizes the *syn* conformation.³¹ Interaction with the protein can also influence the *syn-anti* equilibrium.

Our study showed that a single amino acid can affect the *syn-anti* equilibrium of the nucleotide (Fig. 7). Since nucleotides are usually in the *anti* conformation during base pairing, template-dependent polymerases require a conformational change in the incoming nucleotide from *syn* to *anti* for catalysis.³⁸ The biased conformation of *syn*-dGTP in K263D may have inhibited *syn-anti* conversion and resulted in a lower k_{cat} value compared to the wild type (Table 2 and Table S4).

Incorporation of NTP

NTPs, which are more abundant in the cell than dNTPs, are thought to be potential inhibitors of dNTP-ttPolX binding. However, comparison of the results of our binding study and intracellular concentrations of NTPs may exclude this possibility. The binding affinity of ttPolX for Mg²⁺-GTP was approximately 2 orders lower than that for Mg²⁺-dGTP (Table 1). This difference in binding affinities may be consistent with the fact that ttPolX can incorporate NTPs in addition to dNTPs, although the polymerase activity for NTPs is lower than that for dNTPs.¹⁵ Kinetic and structural studies of Pol β revealed that Tyr271 at the nucleotide-binding pocket contributes to reject ribonucleotide insertion with steric and geometric effects.³⁹ The backbone carbonyl of Tyr271 is clashed with the 2'-OH of the ribonucleotides, and the side chain of Tyr271 adjusts its catalytic positioning by interaction with the primer terminus. The conservation of this tyrosine in ttPolX (Tyr258; Figs. 4d and f, 5, and 6) at the same position as Pol β suggests the same mechanism. In mammalian cells, the intracellular concentration of dNTPs is 5.2–37 μM and that of NTPs is 278–3152 μM .⁴⁰ In other organisms, nucleotide concentrations have been determined by various methods and found to be similar.^{41–43} The ratio of NTP/dNTP in *T. thermophilus* cultured in synthetic medium was estimated as approximately 10.6:1 for CTP/dCTP and 154:1 for ATP/dATP from metabolomics data;⁴⁴ these values are again similar to those of other organisms.^{40,41,43} The ratio of the K_{d} of GTP/dGTP of ttPolX is $\sim 100:1$ (Table 1); therefore, we conclude that ttPolX is mainly bound to metal ion-dNTP and not NTP in cells.

Single-nucleotide gap filling of ttPolX

This study has identified the strategy used by ttPolX for filling 1-nt gaps (summarized in Fig. 10). Biochemical and crystallographic studies revealed that Lys263 in ttPolX contributed to the strong binding affinity for Mg²⁺-dNTP in the absence of DNA with binding to both *syn*- and *anti*-dNTPs (Figs. 4, 7, and 8; Table 1). Steady-state kinetic approach and inhibition assays showed that ttPolX followed a dNTP-first Theorell-Chance mechanism

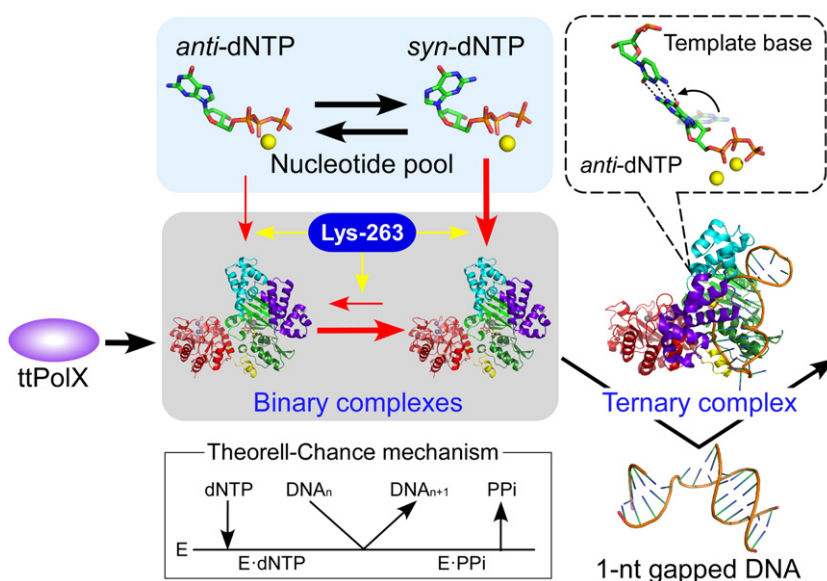


Fig. 10. A model for efficient 1-nt gap filling by ttPolX. In solution, dNTPs are in equilibrium between the *syn* and *anti* conformations. ttPolX can bind both Mg^{2+} -*syn*-dNTP and Mg^{2+} -*anti*-dNTP in the absence of DNA. The dNTP bound to ttPolX may change its conformation between *syn* and *anti*, but the proportion with an *anti* conformation is small (Fig. 4e). This *syn-anti* equilibrium may be modulated by Lys263 and may contribute to the stability of the binary complex in the absence of DNA. In the presence of DNA, the bound *syn*-dNTP changes its conformation to *anti* and base pairs

with the DNA. dNTP-bound ttPolX reacts with 1-nt gapped DNA in a “hit-and-run” fashion via a Theorell–Chance mechanism.

for filling 1-nt gaps (Fig. 3 and Table 2). This mechanism is thought to be a special case of an ordered Bi Bi mechanism with low concentration of the ternary complex under steady-state conditions. It was reported that the reaction mechanism of mouse DNA polymerase α , a replicative polymerase with moderate processivity, was close to a Theorell–Chance mechanism with DNA as the first substrate.⁴⁵ Theorell–Chance mechanisms may be a common strategy for the efficient catalysis of template-dependent polymerases, regardless of whether the first substrate is dNTP or DNA. Our observations here raise the question of how dNTP-bound ttPolX fills 1-nt gaps with the four template bases. In the case of ASFV PolX, dNTP-bound PolX had low affinity against primer/template DNA with mismatched template.³ The dNTP-first binding of ttPolX indicates that it has the same mechanism for gapped DNA. In conclusion, ttPolX may form four dNTP–ttPolX binary complexes for 1-nt gaps with different templates in the cell.

Materials and Methods

Materials

The dNTPs were from Sigma, St Louis, MO, USA. The DNA oligomers were synthesized by BEX Co., Tokyo, Japan. All other reagents used were of the highest grade and commercially available.

Protein overexpression and purification

Overexpression and purification of ttPolX (ORF ID, TTHA1150) were performed as described previously.¹⁵

For expression of selenomethionyl ttPolX, *E. coli* B834(DE3) cells carrying pET-11a/ttPolX and pRARE (Novagen) were cultured in LB medium at 37 °C to a density of 1×10^8 cells/ml. Cells were harvested, resuspended in LeMaster medium⁴⁶ (containing L-selenomethionine) and lactose, and cultured at 37 °C for 24 h. Purification of selenomethionyl ttPolX was performed in the same way as for native ttPolX. We obtained 1.5 g (wet weight) of cells expressing selenomethionyl ttPolX and 1 mg of purified selenomethionyl ttPolX. The pET-11a/ttPolX plasmid was used as a template to generate Lys263 mutants by means of the inverse PCR method using the following primers: 5'-CGGCCACTCCATCCGCTTC-3' (K263A, forward), 5'-ACGCCACTCCATCCGCTTC-3' (K263D, forward), and 5'-CGTCCCCGTGAGGTACTG-GAGG-3' (K263A and K263D, reverse). PCR was performed using KOD -Plus- Ver. 2 DNA polymerase (TOYOBO, Osaka, Japan) and low amount of the template plasmid (<1 ng). The targeted fragments were electrophoresed and purified from the gel. Purified fragments were mixed with DpnI, T4 polynucleotide kinase, and ATP in the T4 DNA ligase buffer. After incubation at 37 °C for 30 min, the solution was mixed with T4 DNA ligase and incubated at 16 °C overnight. The self-ligated plasmids were amplified using *E. coli* DH5 α . The expression and purification of Lys263 mutants were performed similar to those of the wild type.

Surface plasmon resonance

SPR analysis was performed at 25 °C using a Biacore3000 (GE Healthcare UK Ltd., England). ttPolX was diluted with 10 mM acetate (pH 6.0) to 0.1 mg/ml and immobilized on a CM4 sensor chip by amine coupling followed by blocking with ethanolamine hydrochloride. Approximately 7000–10,000 resonance units (RU) of ttPolXs were immobilized. Since dNTPs have low molecular weight (~500) and are difficult to detect, as much ttPolX as possible was immobilized. Control cells were

also blocked by ethanolamine hydrochloride in a similar manner to ttPolX cells to reduce nonspecific electrostatic binding. The running buffer was composed of 10 mM Hepes–NaOH, 100 mM KCl, and 10 mM MgCl₂ or CaCl₂, pH 7.5, and was filtered and degassed. The concentrations of nucleotides were determined by extinction coefficients.⁴⁷ Each nucleotide diluted with running buffer was injected over ttPolX at flow rates of 30–100 μl/min. After binding for 2.5–5 min, ttPolX–nucleotide complexes were dissociated using running buffer without nucleotides, followed by flowing running buffer without metal ions. Experiments with *T. thermophilus* HB8 PolI (ttPolI) were performed in the same manner as for ttPolX. We failed in our attempts to measure the kinetic parameters of binding because the level of immobilization was too high. Therefore, the dissociation constant (K_d) was calculated by fitting the average RU of the steady state (R_{eq}) to the following equation using Igor 4.03 (WaveMetrics, Oregon, USA):

$$R_{eq} = R_{max} [S] / ([S] + K_d) \quad (1)$$

where R_{eq} and R_{max} correspond to [ES] and $[E]_0$, respectively, and [S] is the free concentration of nucleotides. The observed R_{max} was much lower than the theoretical R_{max} [=immobilized ttPolX (RU) × binding ratio (=1) × MW of nucleotide/MW of ttPolX] because ttPolX was probably inactivated either by the immobilization buffer (10 mM acetate, pH 6.0) or by immobilization at more than two points. Another possibility is that immobilization at the POLXc domain inhibited nucleotide binding. We purified and immobilized the POLXc domain (residues 1–316 of ttPolX) and obtained a barely discernable SPR response upon flow of Mg²⁺-dGTP.

DNA polymerase assay

The sequence of oligonucleotides were 5'-ATGACAACTAAAGCAACACCC-3' (21-mer primer), 5'-ATGACAACTAAAGCAACACCCG-3' (22-mer primer), 5'-CACTGGCGGTCGTTCTATCGGGTGTTCGTT-TAGTTGTCAT-3' (40-mer template), and 5'-pATA-GAACGACCGCCAGTG-3' (5'-phosphorylated 18-mer downstream). The 5'-end of the 21-mer primer was radiolabeled using [γ -³²P]ATP and T4 polynucleotide kinase and purified by ethanol precipitation. Oligonucleotides were mixed in the primer:template ratio of 1:1.2 (primer/template) or the primer:template:downstream ratio of 1:1.2:1.5 (1-nt gap and nick). Mixed oligonucleotides in buffer containing 1 mM Tris–HCl (pH 7.5), 0.1 mM ethylenediaminetetraacetic acid (pH 8.0), and 100 mM KCl were heated at 95 °C for 2 min and cooled gradually to allow annealing. For 1-nt gap-filling assay, a reaction mixture was typically composed of 50 mM Tris–HCl, 100 mM KCl, 10 mM MgCl₂, 100 μg/ml bovine serum albumin (BSA), 0.00625–10 μM dGTP, and 2–500 nM annealed 1-nt gapped DNA, pH 7.5°, at 37 °C. The reaction was initiated by adding 0.5–20 nM ttPolX wild type or mutants. The samples were analyzed by 20% (w/v) denaturing PAGE (8 M urea) and visualized by autoradiography using BAS2500 (Fuji Film). For inhibition assay, dCTP (mismatched substrate), pyrophosphate (PPi) (Sigma, USA), and nicked DNA were used as inhibitors. The apparent rate constant k_{app} ($=v_0/[E]_0$) was plotted

against [S] and [I] and fitted to the following equations using Igor 4.03 (WaveMetrics):

$$k_{app} = k_{cat}[S] / (K_m + [S]) \text{ (no inhibition)} \quad (2)$$

$$k_{app} = k_{cat}[S] / ((1 + [I]/K_i)K_m + [S]) \text{ (competitive inhibition)} \quad (3)$$

$$k_{app} = k_{cat}[S] / ((1 + [I]/K_i)K_m + (1 + [I]/K'_i)[S]) \text{ (mixed inhibition)} \quad (4)$$

where v_0 , $[E]_0$, [S], [I], k_{cat} , and K_m are initial velocity, total enzyme concentration, free substrate concentration, free inhibitor concentration, catalytic rate constant, and Michaelis constant, respectively. K_i and K'_i are inhibition constants for binding to different enzyme species.

Crystal structure analysis

Native or selenomethionyl ttPolX with dGTP were crystallized by the hanging-drop vapor-diffusion method with seeding. Drops (1 μl) of 5 mg/ml ttPolX containing 1 mM dGTP were mixed with 1 μl of crystallization solution containing 0.2 M potassium chloride, 0.01 M calcium chloride, 0.005 M sodium cacodylate (pH 6.0), and 5% or 10% polyethylene glycol 4000 (v/v) and equilibrated against 0.15 ml of the reservoir solution at 20 °C. A few days later, highly clustered crystals were broken up and diluted with the reservoir solution. Protein solutions with dGTP were mixed with the seed solution and crystallized as above. The crystals were grown at 20 °C for about 9 months (native ttPolX) or a few days (selenomethionyl ttPolX) to obtain large crystals. Crystallization of the Lys263 mutants was performed similarly to the wild type but without seeding. For crystallization of the ternary complex of ttPolX with 1-nt gapped DNA and Mg²⁺-ddGTP, a DNA 28-mer (pGCCGTTTTTCGGCCCCGACTGTTTTTCAGTC) was self-annealed in 10 mM Tris–HCl (pH 7.5), 100 mM KCl, and 15 mM MgCl₂ using a thermal cycler by heating for 10 min at 90 °C and cooling to 4 °C (1 °C/min). Annealed 2-nt gapped loop DNA (200 μM) was incubated with ttPolX (100 μM) and ddGTP (1 mM) (GE Healthcare UK Ltd.) at 20 °C overnight to make 1-nt gapped DNA. The resultant mixture (1 μl) was mixed with 1 μl 15% polyethylene glycol 1500 (v/v) and crystallized as above. For crystallization of the ttPolX with primer/template and Mg²⁺-ddGTP complex, template (CGGCCATACTG) and primer (CAGTAT) were mixed in a 1:1 ratio in 40 mM Tris–HCl (pH 7.5) and 10 mM MgCl₂ and annealed using a thermal cycler as above. The annealed primer/template DNA was mixed with ttPolX and ddGTP, resulting in 200 μM DNA, 100 μM (6.4 mg/ml) ttPolX, and 1 mM ddGTP. After incubation at 20 °C overnight, the solution was mixed with 50 mM Tris–HCl (pH 8.5), 25 mM MgSO₄·7H₂O, and 1.8 M ammonium sulfate and crystallized as above. For cryoprotection, drops (2 μl) containing the crystals were mixed with 5 μl of crystallization solution containing 22.5% ethylene glycol (v/v), and then 5 μl of mixed solution was removed. This manipulation was repeated at least three times, and then the crystals were

flash-frozen in a liquid nitrogen stream (-180°C). Selenium multiple-wavelength anomalous dispersion data and other single-wavelength diffraction data were collected at beamline BL26B2^{48–51} at SPring-8 (Hyogo, Japan).

The data were processed by the HKL2000 program package.⁵² Of 10 selenium sites, 7 were determined with the program SOLVE.⁵³ The resulting phases were improved with the program RESOLVE,^{54,55} followed by automatic model tracing with the program ARP/wARP.⁵⁶ Model refinement was carried out initially for the selenomethionyl ttPolX diffraction data and continued for the native ttPolX diffraction data using the following programs: CCP4 suite, XtalView/X-fit, Coot, CNS, and Refmac5.^{57–62} The occupancy of *syn* and *anti* conformations of dGTP was refined by a program of PHENIX.⁶³ The stereochemistry of the structure was checked using the program PROCHECK.⁶⁴ Data collection and refinement statistics are shown in Table 3.

Accession numbers

The atomic coordinates have been deposited in the Protein Data Bank (IDs: 3AU2, 3AU6, 3AUO, 3B0X, and 3BOY).

Acknowledgements

We thank Mr. Masao Inoue for helpful discussion. We also thank Mr. Hirofumi Omori for DNA sequencing. The synchrotron radiation experiments were performed at BL26B2 in SPring-8 with the approval of RIKEN (Proposal No. 20110005). This work was supported by Grants-in-Aid for Scientific Research 20570131 (R. Masui) and 19770083 (N. Nakagawa) from the Ministry of Education, Science, Sports, and Culture of Japan, and the Japan Society for the Promotion of Science for Young Scientists (22–37, S. Nakane).

Supplementary Data

Supplementary data to this article can be found online at [doi:10.1016/j.jmb.2012.01.025](https://doi.org/10.1016/j.jmb.2012.01.025)

References

- Xu, G., Herzig, M., Rotrekl, V. & Walter, C. A. (2008). Base excision repair, aging and health span. *Mech. Ageing Dev.* **129**, 366–382.
- Oliveros, M., Yañez, R. J., Salas, M. L., Salas, J., Viñuela, E. & Blanco, L. (1997). Characterization of an African swine fever virus 20-kDa DNA polymerase involved in DNA repair. *J. Biol. Chem.* **272**, 30899–30910.
- Kumar, S., Bakhtina, M. & Tsai, M. D. (2008). Altered order of substrate binding by DNA polymerase X from African swine fever virus. *Biochemistry*, **47**, 7875–7887.
- Boule, J. B., Rougeon, F. & Papanicolaou, C. (2001). Terminal deoxynucleotidyl transferase indiscriminately incorporates ribonucleotides and deoxyribonucleotides. *J. Biol. Chem.* **276**, 31388–31393.
- Deibel, M. R. & Coleman, M. S. (1980). Biochemical properties of purified human terminal deoxynucleotidyltransferase. *J. Biol. Chem.* **255**, 4206–4212.
- McClure, W. R. & Jovin, T. M. (1975). Steady state kinetic parameters and non-processivity of *Escherichia coli* deoxyribonucleic acid polymerase I. *J. Biol. Chem.* **250**, 4073–4080.
- Muise, O. & Holler, E. (1985). Interaction of DNA polymerase I of *Escherichia coli* with nucleotides antagonistic effects of single-stranded polynucleotide homopolymers. *Biochemistry*, **24**, 3618–3622.
- Bryant, F. R., Johnson, K. A. & Benkovic, S. J. (1983). Elementary steps in the DNA polymerase I reaction pathway. *Biochemistry*, **22**, 3537–3546.
- Tanabe, K., Bohn, E. W. & Wilson, S. H. (1979). Steady state kinetics of mouse DNA polymerase β . *Biochemistry*, **18**, 3401–3406.
- Wang, T. S. F. & Korn, D. (1982). Specificity of the catalytic interaction of human DNA polymerase β with nucleic acid substrates. *Biochemistry*, **21**, 1597–1608.
- Beese, L. S., Friedman, J. M. & Steitz, T. A. (1993). Crystal structures of the Klenow fragment of DNA polymerase I complexed with deoxynucleoside triphosphate and pyrophosphate. *Biochemistry*, **32**, 14095–14101.
- Li, Y., Kong, Y., Korolev, S. & Waksman, G. (1998). Crystal structures of the Klenow fragment of *Thermus aquaticus* DNA polymerase I complexed with deoxyribonucleoside triphosphates. *Protein Sci.* **7**, 1116–1123.
- Sawaya, M. R., Pelletier, H., Kumar, A., Wilson, S. H. & Kraut, J. (1994). Crystal structure of rat DNA polymerase β : evidence for a common polymerase mechanism. *Science*, **264**, 1930–1935.
- Delarue, M., Boule, J. B., Lescar, J., Expert-Bezançon, N., Jourdan, N., Sukumar, N. *et al.* (2002). Crystal structures of a template-independent DNA polymerase: murine terminal deoxynucleotidyltransferase. *EMBO J.* **21**, 427–439.
- Nakane, S., Nakagawa, N., Kuramitsu, S. & Masui, R. (2009). Characterization of DNA polymerase X from *Thermus thermophilus* HB8 reveals the POLXc and PHP domains are both required for 3′–5′ exonuclease activity. *Nucleic Acids Res.* **37**, 2037–2052.
- Cleland, W. W. (1963). The kinetics of enzyme-catalyzed reactions with two or more substrates or products. I. Nomenclature and rate equations. *Biochim. Biophys. Acta*, **67**, 104–137.
- Leulliot, N., Cladiere, L., Lecoindre, F., Durand, D., Hubscher, U. & van Tilbeurgh, H. (2009). The family X DNA polymerase from *Deinococcus radiodurans* adopts a non-standard extended conformation. *J. Biol. Chem.* **284**, 11992–11999.
- Chenna, R., Sugawara, H., Koike, T., Lopez, R., Gibson, T. J., Higgins, D. G. & Thompson, J. D. (2003). Multiple sequence alignment with the Clustal series of programs. *Nucleic Acids Res.* **31**, 3497–3500.
- Gouet, P., Robert, X. & Courcelle, E. (2003). ESPript/ENDscript: extracting and rendering sequence and

- 3D information from atomic structures of proteins. *Nucleic Acids Res.* **31**, 3320–3323.
20. Sucato, C. A., Upton, T. G., Kashemirov, B. A., Batra, V. K., Martinek, V., Xiang, Y. *et al.* (2007). Modifying the β,γ leaving-group bridging oxygen alters nucleotide incorporation efficiency, fidelity, and the catalytic mechanism of DNA polymerase β . *Biochemistry*, **46**, 461–471.
21. Holm, L. & Park, J. (2000). DaliLite workbench for protein structure comparison. *Bioinformatics*, **16**, 566–567.
22. Banos, B., Lazaro, J. M., Villar, L., Salas, M. & de Vega, M. (2008). Characterization of a *Bacillus subtilis* 64-kDa DNA polymerase X potentially involved in DNA repair. *J. Mol. Biol.* **384**, 1019–1028.
23. Berg, B. J. V., Beard, W. A. & Wilson, S. H. (2001). DNA structure and aspartate 276 influence nucleotide binding to human DNA polymerase β : implication of the identity of the rate-limiting conformational change. *J. Biol. Chem.* **276**, 3408–3416.
24. Yuan, Z., Bailey, T. L. & Teasdale, R. D. (2005). Prediction of protein B-factor profiles. *Proteins*, **58**, 905–912.
25. Garcia-Diaz, M., Bebenek, K., Larrea, A. A., Havener, J. M., Perera, L., Krahn, J. M. *et al.* (2009). Template strand scrunching during DNA gap repair synthesis by human polymerase λ . *Nat. Struct. Mol. Biol.* **16**, 967–972.
26. Ferrin, L. J. & Mildvan, A. S. (1985). Nuclear Overhauser effect studies of the conformations and binding site environments of deoxynucleoside triphosphate substrates bound to DNA polymerase I and its large fragment. *Biochemistry*, **24**, 6904–6913.
27. Li, Y., Korolev, S. & Waksman, G. (1998). Crystal structures of open and closed forms of binary and ternary complexes of the large fragment of *Thermus aquaticus* DNA polymerase I: structural basis for nucleotide incorporation. *EMBO J.* **17**, 7514–7525.
28. Golosov, A. A., Warren, J. J., Beese, L. S. & Karplus, M. (2010). The mechanism of the translocation step in DNA replication by DNA polymerase I: a computer simulation analysis. *Structure*, **18**, 83–93.
29. Danyluk, S. S. & Hruska, F. E. (1968). Effect of pH upon nuclear magnetic resonance spectra of nucleosides and nucleotides. *Biochemistry*, **7**, 1038–1043.
30. Schweize, M. P., Broom, A. D., Tso, P. O. P. & Hollis, D. P. (1968). Studies of inter- and intramolecular interaction in mononucleotides by proton magnetic resonance. *J. Am. Chem. Soc.* **90**, 1042–1055.
31. Son, T. D., Gueron, M. & Guschlbau, W. (1972). Flexibility and conformations of guanosine monophosphates by Overhauser effect. *J. Am. Chem. Soc.* **94**, 7903–7911.
32. Stolarski, R., Hagberg, C. E. & Shugar, D. (1984). Studies on the dynamic *syn-anti* equilibrium in purine nucleosides and nucleotides with the aid of ^1H and ^{13}C NMR spectroscopy. *Eur. J. Biochem.* **138**, 187–192.
33. Miles, D. W., Robins, M. J., Robins, R. K., Winkley, M. W. & Eyring, H. (1969). Circular dichroism of nucleoside derivatives. V. Cytosine derivatives. *J. Am. Chem. Soc.* **91**, 831–838.
34. Miles, D. W., Townsend, L. B., Robins, M. J., Robins, R. K., Inskip, W. H. & Eyring, H. (1971). Circular dichroism of nucleoside derivatives. X. Influence of solvents and substituents upon Cotton effects of guanosine derivatives. *J. Am. Chem. Soc.* **93**, 1600–1608.
35. Saran, A., Perahia, D. & Pullman, B. (1973). Molecular orbital calculations on conformation of nucleic-acids and their constituents. VII. Conformation of sugar ring in β -nucleosides pseudorotational representation. *Theor. Chim. Acta*, **30**, 31–44.
36. Tso, P. O. P., Kondo, N. S., Schweize, M. P. & Hollis, D. P. (1969). Studies of conformation and interaction in dinucleoside mono- and diphosphates by proton magnetic resonance. *Biochemistry*, **8**, 997–1029.
37. Ikehara, M., Uesugi, S. & Yoshida, K. (1972). Studies on conformation of purine nucleosides and their 5'-phosphates. *Biochemistry*, **11**, 830–836.
38. Kapuler, A. M. & Reich, E. (1971). Some stereochemical requirements of *Escherichia coli* ribonucleic acid polymerase. Interaction with conformationally restricted ribonucleoside 5'-triphosphates: 8-bromoguanosine, 8-ketoguanosine, and 6-methylcytidine triphosphates. *Biochemistry*, **10**, 4050–4061.
39. Cavanaugh, N. A., Beard, W. A., Batra, V. K., Perera, L., Pedersen, L. G. & Wilson, S. H. (2011). Molecular insights into DNA polymerase deterrents for ribonucleotide insertion. *J. Biol. Chem.* **286**, 31650–31660.
40. Traut, T. W. (1994). Physiological concentrations of purines and pyrimidines. *Mol. Cell. Biochem.* **140**, 1–22.
41. Bochner, B. R. & Ames, B. N. (1982). Complete analysis of cellular nucleotides by two-dimensional thin-layer chromatography. *J. Biol. Chem.* **257**, 9759–9769.
42. Soga, T., Ueno, Y., Naraoka, H., Matsuda, K., Tomita, M. & Nishioka, T. (2002). Pressure-assisted capillary electrophoresis electrospray ionization mass spectrometry for analysis of multivalent anions. *Anal. Chem.* **74**, 6224–6229.
43. Buckstein, M. H., He, J. & Rubin, H. (2008). Characterization of nucleotide pools as a function of physiological state in *Escherichia coli*. *J. Bacteriol.* **190**, 718–726.
44. Ooga, T., Ohashi, Y., Kuramitsu, S., Koyama, Y., Tomita, M., Soga, T. & Masui, R. (2009). Degradation of ppGpp by nudix pyrophosphatase modulates the transition of growth phase in the bacterium *Thermus thermophilus*. *J. Biol. Chem.* **284**, 15549–15556.
45. Tanabe, K., Taguchi, Y. N., Matsukage, A. & Takahashi, T. (1980). Steady-state kinetics of mouse DNA polymerase α . *J. Biochem.* **88**, 35–38.
46. LeMaster, D. M. & Richards, F. M. (1985). ^1H - ^{15}N heteronuclear NMR studies of *Escherichia coli* thiorodoxin in samples isotopically labeled by residue type. *Biochemistry*, **24**, 7263–7268.
47. Struhl, K. (2001). Reagents and radioisotopes used to manipulate nucleic acids. *Curr. Protoc. Mol. Biol.* Chapter 3: Unit 3.4.
48. Ueno, G., Hirose, R., Ida, K., Kumasaka, T. & Yamamoto, M. (2004). Sample management system for a vast amount of frozen crystals at SPring-8. *J. Appl. Crystallogr.* **37**, 867–873.
49. Ueno, G., Kanda, H., Kumasaka, T. & Yamamoto, M. (2005). Beamline Scheduling Software: administration software for automatic operation of the RIKEN structural genomics beamlines at SPring-8. *J. Synchrotron Radiat.* **12**, 380–384.
50. Ueno, G., Kanda, H., Hirose, R., Ida, K., Kumasaka, T. & Yamamoto, M. (2006). RIKEN structural genomics

- beamlines at the SPring-8; high throughput protein crystallography with automated beamline operation. *J. Struct. Funct. Genomics*, **7**, 15–22.
51. Okazaki, N., Hasegawa, K., Ueno, G., Murakami, H., Kumasaka, T. & Yamamoto, M. (2008). Mail-in data collection at SPring-8 protein crystallography beamlines. *J. Synchrotron Radiat.* **15**, 288–291.
 52. Otwinowski, Z. & Minor, W. (1997). Processing of X-ray diffraction data collected in oscillation mode. *Methods Enzymol.* **276**, 307–326.
 53. Terwilliger, T. C. & Berendzen, J. (1999). Automated MAD and MIR structure solution. *Acta Crystallogr., Sect. D: Biol. Crystallogr.* **55**, 849–861.
 54. Terwilliger, T. C. (2000). Maximum-likelihood density modification. *Acta Crystallogr., Sect. D: Biol. Crystallogr.* **56**, 965–972.
 55. Terwilliger, T. C. (2003). Automated main-chain model building by template matching and iterative fragment extension. *Acta Crystallogr., Sect. D: Biol. Crystallogr.* **59**, 38–44.
 56. Langer, G., Cohen, S. X., Lamzin, V. S. & Perrakis, A. (2008). Automated macromolecular model building for X-ray crystallography using ARP/wARP version 7. *Nat. Protoc.* **3**, 1171–1179.
 57. Bailey, S. (1994). The CCP4 suite: programs for protein crystallography. *Acta Crystallogr., Sect. D: Biol. Crystallogr.* **50**, 760–763.
 58. McRee, D. E. (1999). XtalView Xfit—a versatile program for manipulating atomic coordinates and electron density. *J. Struct. Biol.* **125**, 156–165.
 59. Emsley, P. & Cowtan, K. (2004). Coot: model-building tools for molecular graphics. *Acta Crystallogr., Sect. D: Biol. Crystallogr.* **60**, 2126–2132.
 60. Brunger, A. T., Adams, P. D., Clore, G. M., DeLano, W. L., Gros, P., Grosse-Kunstleve, R. W. *et al.* (1998). Crystallography & NMR system: a new software suite for macromolecular structure determination. *Acta Crystallogr., Sect. D: Biol. Crystallogr.* **54**, 905–921.
 61. Brunger, A. T. (2007). Version 1.2 of the crystallography and NMR system. *Nat. Protoc.* **2**, 2728–2733.
 62. Vagin, A. A., Steiner, R. A., Lebedev, A. A., Potterton, L., McNicholas, S., Long, F. & Murshudov, G. N. (2004). REFMAC5 dictionary: organization of prior chemical knowledge and guidelines for its use. *Acta Crystallogr., Sect. D: Biol. Crystallogr.* **60**, 2184–2195.
 63. Adams, P. D., Afonine, P. V., Bunkoczi, G., Chen, V. B., Davis, I. W., Echols, N. *et al.* (2010). PHENIX: a comprehensive Python-based system for macromolecular structure solution. *Acta Crystallogr., Sect. D: Biol. Crystallogr.* **66**, 213–221.
 64. Laskowski, R. A., Macarthur, M. W., Moss, D. S. & Thornton, J. M. (1993). PROCHECK: a program to check the stereochemical quality of protein structures. *J. Appl. Crystallogr.* **26**, 283–291.
 65. Eisenberg, D., Schwarz, E., Komaromy, M. & Wall, R. (1984). Analysis of membrane and surface protein sequences with the hydrophobic moment plot. *J. Mol. Biol.* **179**, 125–142.